JOURNAL OF APPLIED PHYSICS **103**, 123530 (2008)

Phosphorus incorporation during Si(001):P gas-source molecular beam epitaxy: Effects on growth kinetics and surface morphology

B. Cho,[a] J. Bareño, Y. L. Foo,[b] S. Hong,[c] T. Spila, I. Petrov, and J. E. Greene[d]
Materials Science Department and the Frederick-Seitz Materials Research Laboratory, University of Illinois, 104 South Goodwin Ave., Urbana, Illinois 61801, USA

(Received 12 November 2007; accepted 14 March 2008; published online 25 June 2008)

The effects of P doping on growth kinetics and surface morphological evolution during Si(001):P gas-source molecular beam epitaxy from Si_2H_6 and PH_3 at temperatures $T_s = 500-900$ °C have been investigated. With increasing PH_3/Si_2H_6 flux ratio $J_{P/Si}$ at constant T_s, we observe a decrease in the film growth rate R and an increase in the incorporated P concentration C_P, both of which tend toward saturation at high flux ratios, which is accompanied by increased surface roughening and pit formation. At constant $J_{P/Si}$, R increases with increasing T_s, while C_P initially increases, reaches a maximum at $T_s = 700$ °C, and then decreases at higher growth temperatures. We use *in situ* isotopically tagged D_2 temperature programed desorption (TPD) to follow changes in film surface composition and dangling bond density θ_{db} as a function of $J_{P/Si}$ and T_s. Measurements are carried out on both as-deposited Si(001):P layers and P-adsorbed Si(001) surfaces revealing β_1 and β_2 peaks due to D_2 desorption from Si monohydride and dihydride species, respectively, as well as the formation of a third peak β_3 corresponding to D_2 desorption from mixed Si—P dimers. Dissociative PH_3 adsorption on Si(001) results in a decrease in θ_{db} and an initial increase in P surface coverage θ_P with increasing T_s. Saturation θ_P values reach a maximum of ~1 ML at $T_s = 550$ °C, and decrease with $T_s > 600$ °C due to the onset of P_2 desorption. Comparison of $\theta_P(T_s)$ results obtained during film growth with postdeposition $C_P(T_s)$ results reveals the presence of strong P surface segregation. From measurements of θ_P versus C_P in Si(001):P layers grown as a function of T_s, we obtain a P segregation enthalpy $\Delta H_s = -0.86$ eV. By using the combined set of results, we develop a predictive model for C_P versus T_s and, $J_{P/Si}$ incorporating the dependence of the PH_3 reactive sticking probability S_{PH_3} on θ_P, which provides an excellent fit to the experimental data. © *2008 American Institute of Physics*. [DOI: 10.1063/1.2925798]

I. INTRODUCTION

Phosphorus is a common *n*-type dopant in Si-based microelectronic devices, typically introduced during Si(001):P chemical vapor deposition (CVD) by using PH_3 as a precursor. However, P exhibits a strong tendency toward surface segregation[1] and, due to its pentavalent nature, terminates Si(001) surface dangling bonds. This, in turn, influences the Si(001):P film growth rate[2,3] and induces surface roughening.[4,5] The observed decrease in growth rate and the onset of surface roughening are directly related to the presence of P at the growth surface. Thus, quantitative measurements of the P surface coverage θ_P as a function of deposition conditions, which include incident precursor fluxes and film growth temperature T_s, are essential for understanding the effects of P doping on the growth of epitaxial Si(001) and for modeling P incorporation kinetics.

In this article, we present the results of experiments—which utilize a combination of *in situ* D_2 temperature programed desorption (TPD), Auger electron spectroscopy (AES), and reflection high-energy electron diffraction (RHEED), together with postdeposition atomic force microscopy (AFM), transmission electron microscopy (TEM), high-resolution x-ray diffraction (HR-XRD), and secondary ion mass spectroscopy (SIMS)—designed to determine the P surface coverage θ_P, film growth rate R, incorporated P concentration C_P, and the microstructure and surface morphology of Si(001):P layers versus T_s and the PH_3 flux J_{PH_3}. We then use kinetic rate equations describing the adsorption of PH_3 on Si(001) and the desorption of H_2 and P_2, to formulate an expression for $\theta_P(T_s, J_{PH_3})$. From the combination of steady-state T_s-dependent θ_P and C_P results during Si(001):P film growth, we obtain the P segregation enthalpy, $\Delta H_s = -0.86$ eV, and develop a predictive model for dopant incorporation that expresses C_P as a function of T_s and J_{PH_3}.

Si(001):P layers are grown in ultra-high vacuum (UHV) by gas-source molecular beam epitaxy (GS-MBE) from Si_2H_6 and PH_3. GS-MBE was chosen for these experiments, rather than CVD, in order to use *in situ* TPD and AES for quantitative measurements of surface dangling bond and P coverages as a function of T_s and J_{PH_3}.

II. EXPERIMENTAL PROCEDURE

All Si(001):P films are grown in a multichamber ultrahigh vacuum system, which is described in detail in Ref. 6 and is evacuated by a combination of ion and turbomolecular pumps to a base pressure of 5×10^{-11} Torr. The film growth

[a] Electronic mail: benjamin_cho@emcore.com.
[b] Present address: Institute of Materials Research and Engineering, 3 Research Link, Singapore 117602.
[c] Present address: The School of Chemical and Biomolecular Engineering, Cornell University, Ithaca, New York 14850.
[d] Electronic mail: jegreene@uiuc.edu.

0021-8979/2008/103(12)/123530/10/$23.00

© 2008 American Institute of Physics

Downloaded 07 Oct 2008 to 130.126.103.113. Redistribution subject to AIP license or copyright; see http://jap.aip.org/jap/copyright.jsp

chamber is equipped with RHEED and is connected through a transfer chamber to an analytical chamber containing provisions for AES and low-energy electron diffraction. TPD measurements are performed in a separate chamber containing a heavily differentially pumped Extrel quadrapole mass spectrometer (QMS) connected to the analytical station.

The Si(001) substrates are 1×3 cm^2 plates cleaved from 500-μm-thick *p*-type Si wafers. Initial cleaning consists of solvent degreasing by successive rinses in trichloroethane, acetone, propanol, and de-ionized water. The substrates are then subjected to four wet-chemical oxidation/etch cycles composed of the following steps: 2 min in a 2:1:1 solution of $H_2O:HCl:H_2O_2$, a rinse in fresh ultrapure de-ionized water, and a 30 s etch in dilute (10%) HF. They are blown dry in ultrahigh purity Ar, exposed to a UV/ozone treatment involving UV irradiation from a low-pressure Hg lamp (15 mW cm^{-2}) for 30 min in air to remove C-containing species,[7] and introduced through the transfer chamber into the deposition system where they are degassed at 600 °C for 4 h, followed by flash heating to consecutively higher temperatures, reaching a maximum of 1100 °C, to remove the oxide. The chamber pressure does not exceed 5×10^{-9} Torr during oxide desorption. RHEED patterns from substrates subjected to this procedure are 2×1 with sharp Kikuchi lines. No residual C or O is detected by AES.

Two types of samples are used in these experiments. The first set consists of P-adsorbed Si(001) wafers with surface coverages θ_P=0.12–0.98 ML (ML denotes monolayer) as measured by TPD. The samples are obtained by exposing clean substrates to a PH_3 flux of 1.6×10^{14} cm^{-2} s^{-1} for sufficient time to reach saturation coverage (up to 30 min) at temperatures between 300 and 900 °C. They are then quenched to room temperature at ~100 °C s^{-1}. Based on phosphorus TPD results (Sec. III A and IV A) and the known desorption rate constant (Sec. IV A), the maximum loss in P coverage during quenching from the highest temperature of 900 °C is insignificant, <0.03 ML. P-adsorbed samples are used to determine steady-state $\theta_P(T_s)$ values and provide TPD spectra for comparison with doped Si(001):P layers.

The second set of samples consists of P-doped Si(001) layers, which are ~100 nm thick. These specimens are used for SIMS measurements of the incorporated P concentration C_P, as well as for AFM, TEM, and XRD investigations. The films are grown from Si_2H_6 and PH_3 molecular beams delivered to the substrate through individual directed tubular dosers located 3 cm from the substrate at an angle of 45°. The dosers are coupled to feedback-controlled constant-pressure reservoirs, in which pressures are separately monitored by capacitance manometers whose signals are, in turn, used to control variable leak valves. Valve sequencing, pressure, gas flows, and substrate temperature are all computer controlled. PH_3 to Si_2H_6 flux ratios in these experiments range from 0.002 to 0.161.

Following P adlayer or Si(001):P deposition, the samples are quenched to room temperature and exposed to atomic deuterium until all H is replaced by D and saturation coverage $\theta_{D,sat}$ is achieved. For this purpose, D_2 is delivered through a doser identical to those in the growth chamber and a hot W filament in the gas stream is used to crack the gas. Deuterium is employed rather than hydrogen to suppress the background signal during TPD measurements.

The TPD experiments are performed in the analytical chamber with the sample placed 2 mm from the 5 mm diameter hole in the skimmer cone of the Extrel QMS. Samples are heated by direct current at a linear rate of 2 °C s^{-1}, while the temperature is determined by a thermocouple calibrated using an optical pyrometer.

Deposited film thicknesses are measured by microstylus profilometry, while P concentrations in as-deposited layers are determined using a Cameca IMS-5F SIMS instrument with a 10 keV Cs$^+$ primary ion beam. Quantification to within an experimental uncertainty of 10% is obtained by using P-implanted bulk-Si standards with known P concentrations. Other than intentionally introduced P, the films contain no detectable impurities.

To investigate the crystalline quality of doped Si(001) layers, HR-XRD scans are acquired by using a four-axis diffractometer with a collimating x-ray mirror, a Bartels four-crystal Ge(022) monochromator, and an Euler sample cradle with independent computer-controlled drive of all sample rotation angles. The instrument is capable of positioning samples to within 1 arc s. Cu $K\alpha_1$ radiation (λ =1.540 597 Å), with an angular divergence of <12 arc s and a wavelength spread of $\sim 2\times 10^{-5}$, is incident at an angle ω with respect to the sample surface.

High-resolution, dark-field, and bright-field cross-sectional TEM (XTEM) analyses are performed in a JEOL 2010 LaB_6 microscope operated at 200 kV. Sample preparation and ion thinning follow the procedure described in Ref. 8.

III. EXPERIMENTAL RESULTS

A. P-adsorbed Si(001) samples

Figure 1(a) is a reference D_2 TPD scan from deuterium-saturated Si(001). The spectrum is composed of two peaks: β_1 centered at 515 °C, due to desorption from the 2×1 monodeuteride phase, and β_2 at 405 °C, due to desorption from the 1×1 dideuteride phase.[9] D_2 TPD spectra from Si(001) surfaces dosed to saturation coverages with J_{PH_3} $=1.6\times 10^{14}$ cm^{-2} s^{-1} at T_s values ranging from 300 to 900 °C are shown in Fig. 1(b). With increasing T_s, the integrated intensities under the TPD spectra decrease, reach a minimum at 600 °C, and then increase at higher T_s values.

The TPD spectra in Fig. 1(b) reveal that PH_3 adsorption on Si(001) at $T_s<600$ °C causes a reduction in β_1 intensity, while β_2 tends to increase relative to that of the clean Si(001) TPD spectrum. As discussed in more detail in subsequent sections, the initial decrease in β_1 intensity $I_{\beta 1}$ with increasing T_s arises from a corresponding decrease in the surface dangling bond coverage in the presence of surface P. $I_{\beta 1}$ reaches a minimum at 600 °C and then increases at T_s >600 °C due to phosphorus desorption. The initial increase in β_2 intensity $I_{\beta 2}(T_s)$ in Fig. 1(b) results from a reduction in Si(001)2×1 dideuteride steric hindrance[10] in the presence of surface Si—P and P—P dimers. With increasing T_s, the P-induced effects on steric hindrance are offset by lower surface dangling bond coverages. $I_{\beta 2}(T_s)$ also exhibits a mini-

Downloaded 07 Oct 2008 to 130.126.103.113. Redistribution subject to AIP license or copyright; see http://jap.aip.org/jap/copyright.jsp

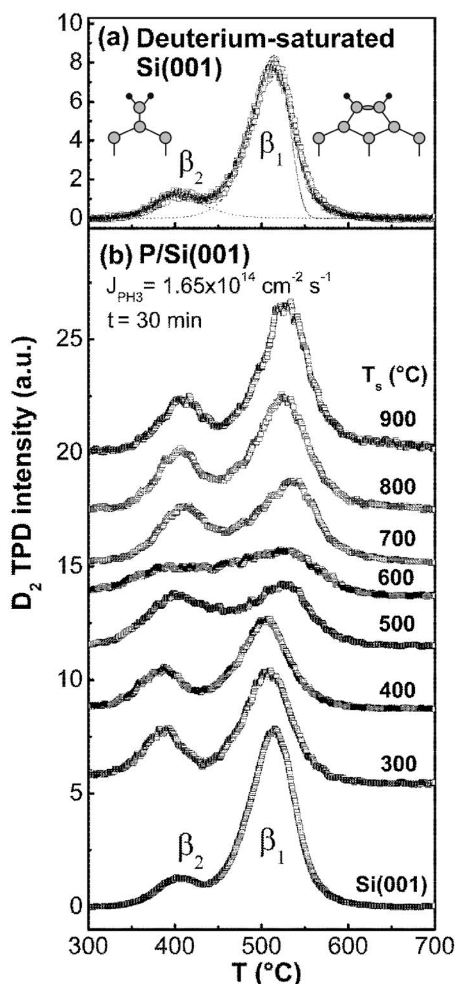

FIG. 1. D_2 TPD spectra from D-saturated (a) Si(001) and (b) Si(001) surfaces exposed to a PH_3 flux $J_{PH_3}=1.65\times10^{14}$ cm^{-2} s^{-1} for 30 min at temperatures T_s of 300–900 °C. The β_1 monodeuteride and β_2 dideuteride surface phases are schematically illustrated in (a). The gray circles correspond to Si atoms, while the black circles are D atoms. Note the strained dimer bond between the upper Si atoms in the β_1 monodeuteride unit.

mum at ~600 °C and increases at higher temperatures as the phosphorus desorption rate becomes significant. Similar TPD results have been reported for As-adsorbed Si(001).[11]

Adsorption of PH_3 on Si(001) yields a surface composed of a mixture of Si—Si, Si—P, and P—P dimers through substitutional incorporation of P adatoms into the first atomic layer of Si(001) via Si atom ejection.[12] P adatoms are pentavalent, forming two bonds to underlying Si atoms and one bond to the neighboring Si (or P) dimer atom. In this bonding state, each P surface atom has a set of lone-pair electrons, rather than a dangling bond (the case for Si surface atoms), as schematically shown in Fig. 2. Thus, the presence of P passivates the surface via a reduction in the dangling bond

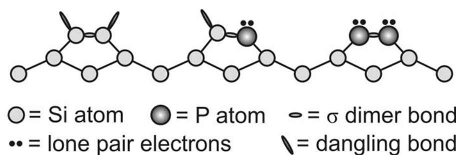

FIG. 2. Schematic representation of Si—Si, Si—P, and P—P dimer bonds on Si(001)2×1 as viewed along the [110] direction.

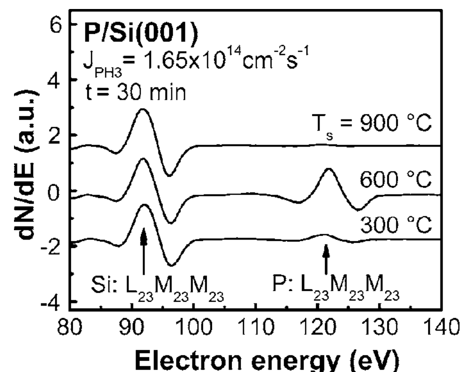

FIG. 3. AES spectra from Si(001) surfaces exposed to a PH_3 flux $J_{PH_3}=1.65\times10^{14}$ cm^{-2} s^{-1} for 30 min at T_s=300, 600, and 900 °C.

density (θ_{db}), which influences the kinetics of layer growth, surface morphological evolution, and dopant incorporation, as will be discussed in Sec. III B and III C.

PH_3 dissociatively adsorbs on Si(001) as PH_2 and H at 100 K, with the onset of PH_2 decomposition occurring at $T_s > 225$ °C.[13] Thus, in our dosing experiments at T_s =300–400 °C, PH_3 decomposes into adsorbed P and three H. Since the H_2 desorption rate at these temperatures is negligible, $\theta_P \sim 0.25$ ML. AES measurements show that θ_P remains constant with increasing T_s until the onset of hydrogen desorption at ~400 °C, above which θ_P increases, reaching a maximum at ~550 °C, and then decreases at T_s >600 °C.[14] The latter is due to the onset of phosphorus desorption as will be discussed later in this section. This behavior is illustrated in Fig. 3, which shows typical AES spectra containing Si and P $L_{23}M_{23}M_{23}$ peaks, located at 92 and 120 eV, respectively, acquired following PH_3 dosing at T_s=300, 600, and 900 °C. The P coverage θ_P increases with T_s from 300 to 600 °C, followed by a decrease in θ_P as T_s is further increased to 900 °C. The ratio between the maximum P AES intensity, obtained at 550 °C, and the 300 °C value, $\theta_{P,max}/\theta_P(300\ °C)$, is approximately 4,[14] indicating that $\theta_{P,max}$ is near 1 ML.

All TPD spectra are fitted by using standard Polanyi–Wigner analysis, in which the desorption rate $d\theta_D/dT$ is expressed as[15]

$$\frac{d\theta_D}{dT} = -\left[\frac{\nu\theta_D{}^n}{\zeta}\right]\exp\left(-\frac{E_a}{kT}\right), \quad (1)$$

where ν is the attempt frequency, θ_D is the instantaneous D coverage, n is the order of the desorption reaction, ζ is the sample heating rate, E_a is the desorption activation energy, and k is the Boltzmann constant. At high pumping speeds,[16]

$$\ln\left[\frac{\theta_D(T)}{\theta_0}\right] = -\frac{\nu}{\zeta}I(T) \quad (2)$$

for first-order desorption, and

$$\theta_D(T) = \frac{\theta_0}{1+\left(\frac{\upsilon}{\zeta}\right)\theta_0 I(T)} \quad (3)$$

for second-order desorption. θ_0 in Eqs.(2) and (3) is the initial coverage and $I(T)$ is given by

Downloaded 07 Oct 2008 to 130.126.103.113. Redistribution subject to AIP license or copyright; see http://jap.aip.org/jap/copyright.jsp

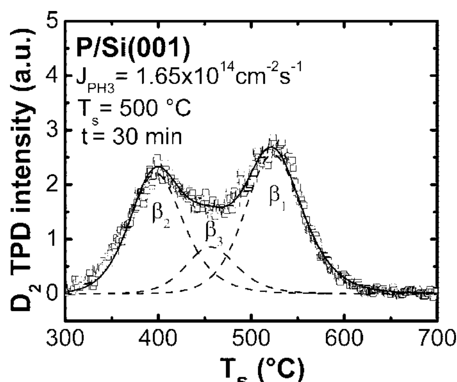

FIG. 4. Fitted D_2 TPD spectra from a Si(001) surface exposed to a PH_3 flux $J_{PH_3}=1.65\times10^{14}$ cm^{-2} s^{-1} for 30 min at $T_s=500$ °C. The spectrum consists of peaks labeled β_1, β_2, and β_3, due to desorption from Si monodeuteride, dideuteride, and mixed Si—P dimers, respectively.

$$I(T)=\frac{E_a}{k}\left|\frac{e^{-\varepsilon}}{\varepsilon^2}\sum_{n=1}^{\infty}\frac{(-1)^{n+1}n!}{\varepsilon^{n-1}}\right|_{T_0}^{T}, \tag{4}$$

in which $\varepsilon=E_a/kT$. Clean Si(001) D_2 TPD spectra (see Fig. 1(a)), are fitted by using second-order desorption for β_2 and first-order desorption for β_1, the latter due to π-bond-induced pairing of D atoms on single dimers.[17] The results yield $E_1=2.52$ eV with $\nu_1=1\times10^{15}$ s^{-1} for β_1 and $E_2=1.88$ eV with $\nu_2=1\times10^{13}$ s^{-1} for β_2, which are consistent with previously reported results.[10] The agreement between measured and calculated spectra is excellent except at high temperatures (i.e., low deuterium coverages), where the measured curve is higher than the calculated curve as D_2 desorption becomes limited by second-order bimolecular recombination.[18] The saturated D coverage ($\theta_{D,sat}$) is 1.2 ML, which is less than the 2 ML expected for complete dideuteride coverage, due to steric hindrance resulting from electronic repulsion between adsorbed nearest-neighbor deuterium atoms.[10]

PH_3 adsorption results, in addition to a decrease in β_1 and an increase in β_2, in the appearance of a new peak β_3 centered at 480 °C. We attribute the emergence of β_3 to deuterium desorption from Si—P heterodimers. D_2 desorption spectra from P-adsorbed Si(001) surfaces are fit using three second-order desorption peaks, as shown in Fig. 4, for a TPD spectrum from a sample dosed with PH_3 at T_s =500 °C. The β_1 and β_2 peaks have the same physical origin as for TPD spectra from clean Si(001), and thus, the same activation energies and frequency factors. However, upon P adsorption, β_1 follows second-order desorption kinetics, as was observed for both Ge- and As-adsorbed Si(001).[11,19] Thus, P adsorption inhibits deuterium pairing on Si(001), presumably due to a reduction in D adatom mobility. The change from first-to second-order desorption kinetics results in the β_1 peak temperature shifting upwards with increasing θ_P (decreasing $\theta_{D,sat}$) as T_s is increased [see Fig. 1(b)]. β_3 is fitted by using the same frequency factor as β_1 but with a slightly lower activation energy of 2.40 eV. Spectra calculated by using Eq. (3) based on the three second-order peaks β_1, β_2, and β_3 are in excellent agreement with all P-adsorbed Si(001) TPD data.

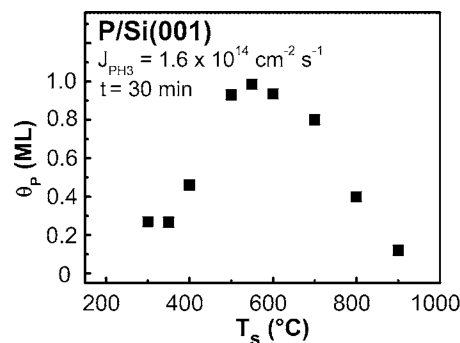

FIG. 5. P coverages θ_P obtained from TPD measurements of Si(001) surfaces exposed to a PH_3 flux $J_{PH_3}=1.65\times10^{14}$ cm^{-2} s^{-1} for 30 min at temperatures T_s between 300 and 900 °C.

From the fitted TPD results, we obtain θ_{db} and θ_P as a function of T_s. The surface dangling bond density can be expressed in terms of the normalized β_1 and β_3 monodeuteride peak intensities as

$$\theta_{db}=\frac{I_{\beta_1}+I_{\beta_3}}{I_{\beta_1,\mathrm{Si}(001)}}, \tag{5}$$

where $I_{\beta_1,\mathrm{Si}(001)}$ is the integrated intensity of the β_1 peak from the clean Si(001) surface. Note that the β_2 intensity is not required in Eq. (5), since the concerted recombinative H_2 desorption from adjacent dihydride species leaves two adjacent Si monohydride units.[20] The P coverage θ_P is then given by the expression

$$\theta_P=1-\theta_{db}=1-\frac{I_{\beta_1}+I_{\beta_3}}{I_{\beta_1,\mathrm{Si}(001)}}. \tag{6}$$

Based on Eqs. (5) and (6), $\theta_{db}=0.87$ ML and $\theta_P=0.13$ ML at $T_s=300$ °C. θ_P then increases (θ_{db} decreases) with increasing T_s, reaching a maximum of 0.49 ML ($\theta_{db}=0.51$ ML) at 550 °C. At higher T_s values, θ_P steadily decreases (θ_{db} increases) to 0.06 ML ($\theta_{db}=0.89$ ML) at $T_s=900$ °C.

The TPD results yield a P coverage ratio $\theta_{P,max}/\theta_P(300$ °C) of ~4 in good agreement with previously reported results[14] based on P AES intensities as well as with our own AES intensity measurements. However, in comparison with the expected θ_P values of ~0.25 ML at T_s =300 °C and ~1 ML at $T_s=550$ °C, the absolute magnitudes of our θ_P results are lower by a factor of 2. We attribute the difference to the presence of P-induced surface defects, previously observed by scanning tunneling microscopy,[12,21,22] which provide additional dangling bond sites for D adsorption and thus cause θ_P values obtained from TPD measurements to underestimate the actual P coverages. To account for this, we insert a factor of 2 in Eq. (6). Thus,

$$\theta_P=2(1-\theta_{db})=2\left(1-\frac{I_{\beta_1}+I_{\beta_3}}{I_{\beta_1,\mathrm{Si}(001)}}\right). \tag{7}$$

Analyses of our TPD data using Eq. (7), which assumes that the surface defect density is linearly proportional to θ_P, yields $\theta_P=0.26$ ML at 300 °C and $\theta_{P,max}=0.98$ ML.

θ_P values obtained by using Eq. (7) are plotted as a function of T_s in Fig. 5. θ_P remains constant at ~0.25 ML up to

Downloaded 07 Oct 2008 to 130.126.103.113. Redistribution subject to AIP license or copyright; see http://jap.aip.org/jap/copyright.jsp

the temperature at which H_2 desorption becomes significant, ~400 °C. θ_P then rapidly increases with T_s, as additional dangling bond sites become available for PH_3 adsorption, and reaches a maximum value of 0.98 ML at T_s=550 °C before decreasing at higher temperatures to 0.12 ML at T_s =900 °C. Our phosphorus TPD results show that the decrease in $\theta_P(T_s)$ is predominantly due to recombinative P_2 desorption, with an onset temperature of ~600 °C. The latter is in agreement with the work of Jacobson *et al.*[23] Saturated $\theta_P(T_s)$ values obtained from P-adsorbed Si(001) samples are used as reference data for analyzing Si(001):P TPD results that will be presented in Sec. III B. The validity of the absolute P coverages we obtain will be further tested and confirmed in Sec. IV C, where we use them to calculate the complete set of P concentrations C_P incorporated in Si(001):P films grown as a function of $J_{P/Si}$ and T_s. The results exhibit good agreement with experimental values.

B. P incorporation and surface coverage during Si(001):P growth

In this section, we use a combination of *in situ* TPD and postdeposition SIMS measurements to determine the steady-state P surface coverage θ_P and the incorporated P concentration C_P as a function of T_s and $J_{P/Si}$ during Si(001):P film growth. The Si(001):P layers, which are ~100 nm thick, are deposited at temperatures ranging from 500 to 900 °C with a constant Si_2H_6 flux of 2.2×10^{16} cm^{-2} s^{-1}; $J_{P/Si}$ is varied from 0.002 to 0.161.

θ_P values were measured as a function of T_s and $J_{P/Si}$ via D_2 TPD by following the procedure discussed in Sec. III A. Typical D_2 TPD scans from P-doped Si(001) layers grown at 800 °C with different values of $J_{P/Si}$ are shown in Fig. 6. The spectra vary with increasing $J_{P/Si}$ in a manner similar to P-adsorbed Si(001) TPD spectra with increasing θ_P [see Fig. 1(b)]: β_1 becomes second order, a new peak β_3 appears, the intensity $I_{\beta1}$ decreases, and both $I_{\beta2}$ and $I_{\beta3}$ increase. The

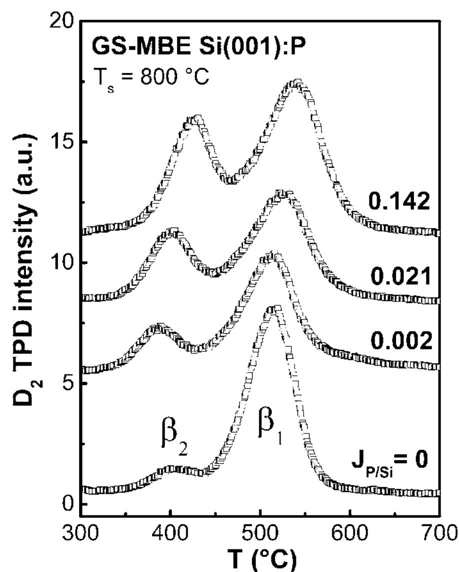

FIG. 6. (a) D_2 TPD spectra from Si(001):P GS-MBE layers grown at T_s =800 °C with incident PH_3/Si_2H_6 flux ratios $J_{P/Si}$ ranging from 0.004 to 0.142. $J_{Si_2H_6}$ is maintained constant at 2.1×10^{16} cm^{-2} s^{-1}.

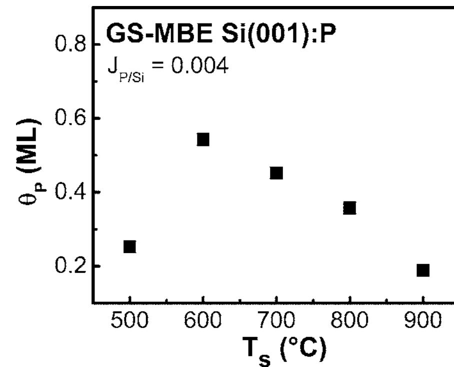

FIG. 7. Steady-state P surface coverages θ_P, which are obtained from TPD measurements during GS-MBE Si(001):P growth at T_s=500–900 °C. The incident PH_3/Si_2H_6 flux ratio is $J_{P/Si}$=0.004.

origins of these changes with $J_{P/Si}$ are identical to those discussed in Sec. III A. in the case of P-adsorbed Si(001). Integrated saturated deuterium coverages $\theta_{D,sat}$ initially decrease with increasing $J_{P/Si}$ due to a P-induced reduction in θ_{db}. However, at high P/Si flux ratios, this effect is offset by surface roughening, which provides additional dangling bonds as will be discussed in Sec. III C.

θ_P versus T_s results for Si(001):P layers grown at constant $J_{P/Si}$ are qualitatively similar to those for P-adsorbed Si(001). Typical data, which in this case are obtained with $J_{P/Si}$=0.004, are plotted in Fig. 7. With increasing T_s, θ_P initially increases, reaches a maximum of 0.54 ML at T_s =600 °C, and then decreases to 0.19 ML at T_s=900 °C.

C_P is plotted as a function of $J_{P/Si}$ and T_s in Fig. 8. At constant T_s, C_P initially increases rapidly with $J_{P/Si}$, and then more slowly at higher PH_3 fluxes. For a given value of $J_{P/Si}$, C_P first increases with T_s up to 700 °C, as the corresponding increase in the hydrogen desorption rate provides more dangling bond sites for PH_3 adsorption, and then decreases at higher T_s values, for which the gain in θ_{db} is overcome by phosphorus loss due to desorption. The maximum C_P is 3.1×10^{19} cm^{-3}, which is obtained at T_s=700 °C with $J_{P/Si}$ =0.142.

The combined results for $\theta_P(T_s,J_{P/Si})$ and $C_P(T_s,J_{P/Si})$ demonstrate strong P surface segregation during Si(001) layer growth. In the absence of surface segregation, θ_P for all Si(001):P layers would be below the TPD detection limit,

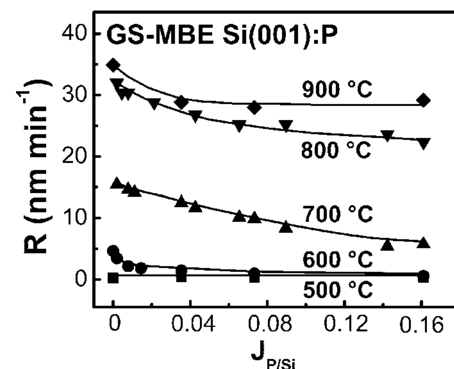

FIG. 8. P concentrations C_P incorporated in GS-MBE Si(001):P layers grown at T_s=500–900 °C with incident PH_3/Si_2H_6 flux ratios $J_{P/Si}$ ranging from 0.004 to 0.161. $J_{Si_2H_6}$ is maintained constant at 2.1×10^{16} cm^{-2} s^{-1}.

Downloaded 07 Oct 2008 to 130.126.103.113. Redistribution subject to AIP license or copyright; see http://jap.aip.org/jap/copyright.jsp

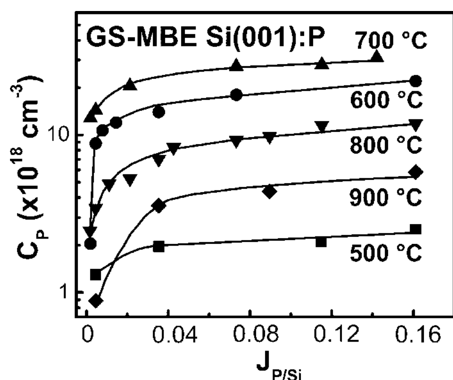

FIG. 9. GS-MBE Si(001):P film growth rates R as a function of the incident PH_3/Si_2H_6 flux ratio $J_{P/Si}$ and deposition temperature T_s. $J_{Si_2H_6}$ is maintained constant at 2.1×10^{16} cm^{-2} s^{-1}.

which is ~0.02 ML. For example, layer growth at $T_s=600$ °C with $J_{P/Si}=0.004$ yields $C_P=8.8\times10^{18}$ cm^{-3} which corresponds to $\theta_P=1.77\times10^{-4}$ ML. However, the actual measured θ_P value is 0.52 ML, which is approximately 3000 times larger.

C. Si(001):P growth rate and surface morphological evolution

Phosphorus surface segregation has a significant effect on the deposition rate R of Si(001):P layers as well as on surface morphological evolution. Film growth kinetics are primarily controlled by the dissociative adsorption rate of Si_2H_6 which strongly varies with θ_H and θ_P whose values are, in turn, highly T_s dependent. Figure 9 is a plot of R versus $J_{P/Si}$ (0–0.161) and T_s (500–900 °C). At $T_s=500$ °C, $R\sim0.34$ nm min^{-1}, which is essentially independent of $J_{P/Si}$ since Si_2H_6 (and PH_3) adsorption is limited by the relatively slow desorption rate of H_2. However, with $T_s\geqslant600$ °C, R decreases with increasing $J_{P/Si}$ due to a corresponding increase in θ_P. At large $J_{P/Si}$, θ_P, and hence R, approach T_s-dependent saturation values. Further increases in $J_{P/Si}$ have little effect on R. Figure 9 also shows that saturation occurs at lower $J_{P/Si}$ values with higher film growth temperatures. At constant $J_{P/Si}$, R increases with T_s due to increasingly rapid H_2 and P_2 desorption. At the highest PH_3 flux used in these experiments ($J_{PH3}=3.40\times10^{15}$ cm^{-2} s^{-1}, $J_{P/Si}=0.161$), R ranges from 0.34 nm min^{-1} at 500 °C to 29.2 nm min^{-1} at 900 °C.

The surface morphological evolution of Si(001):P layers is directly related to the high steady-state P surface coverages resulting from the strong driving force for segregation. Since P terminates surface dangling bond sites and inhibits Si_2H_6 precursor adsorption, instantaneous film growth is inhibited at P surface sites and only occurs at Si sites, which leads to roughening as Si deposition occurs nonuniformly over the surface.

A typical series of AFM images from 100-nm-thick P-doped Si(001) layers grown at $T_s=800$ °C with increasing PH_3 flux is shown in Figs. 10(a)–10(d). At the lowest flux ratio investigated, $J_{P/Si}=0.002$ [Fig. 10(a)], surface roughening proceeds via the formation of ripples along elastically soft ⟨100⟩ directions[24] and small (20–30 nm diameter) Si

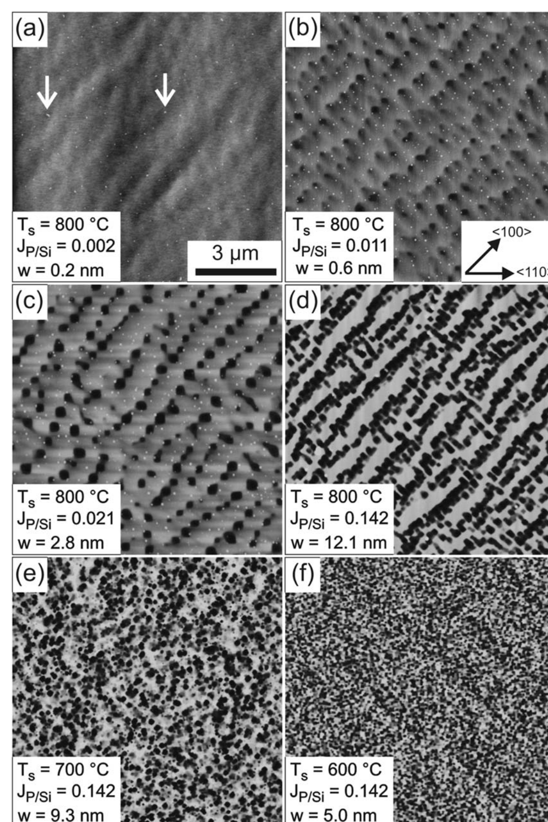

FIG. 10. AFM images of GS-MBE Si(001):P films showing the variation in surface morphology and rms roughness w with growth temperature T_s and incident PH_3/Si_2H_6 flux ratio $J_{P/Si}$: (a) $T_s=800$ °C, $J_{P/Si}=0.002$; (b) 800 °C, 0.011; (c) 800 °C, 0.021; (d) 800 °C, 0.142; (e) 700 °C, 0.142; and (f) 600 °C, 0.142. The white arrows in panel (a) point to small (20–30 nm) Si islands.

islands. The rate of island nucleation during P adsorption is enhanced by the ejection of first-layer Si atoms onto the surface,[12] which raises the Si supersaturation on terraces. Increasing $J_{P/Si}$ to 0.011 gives rise to a larger average Si island size, with a maximum diameter of approximately 100 nm, and the onset of self-organized pit formation aligned along ⟨100⟩ directions [see Fig. 10(b)]. Pits become larger and occupy a higher fraction of the surface area as $J_{P/Si}$ increases [Fig. 10(c)], eventually overlapping at $J_{P/Si}=0.142$, resulting in the formation of ⟨100⟩ oriented trenches [Fig. 10(d)]. The root-mean-square (rms) surface roughness w, shown as an inset in each image, continuously increases with increasing $J_{P/Si}$.

The film growth temperature T_s also has a significant effect on Si(001):P surface morphology due to the interrelated effects of H_2 desorption, P adsorption, P_2 desorption, and kinetic limitations on surface diffusion. This is illustrated by comparing Figs. 10(d)–10(f), which correspond to $T_s=800$, 700, and 600 °C with $J_{P/Si}$ maintained constant at 0.142. The film surface exhibits a spongelike appearance with small pits (average diameter of ~90 nm) at $T_s=600$ °C, while at 700 °C, both pit formation and ordering become more prominent, with an average pit size of ~170 nm. At $T_s=800$ °C self-organized trench structures aligned along ⟨100⟩ are observed. w increases from 5.0 nm at $T_s=600$ °C, to 9.3 nm at $T_s=700$ °C, to 12.1 nm at $T_s=800$ °C.

Downloaded 07 Oct 2008 to 130.126.103.113. Redistribution subject to AIP license or copyright; see http://jap.aip.org/jap/copyright.jsp

No dislocations are observed in XTEM images of even the most highly doped films ($C_P = 3.1 \times 10^{19}$ cm^{-3}) despite the significant degree of P-induced surface roughening observed. 2θ-ω XRD scans of the 004 Bragg peak confirm the high crystalline quality of the highly doped films, with full width at half maximum values $\Gamma_{2\theta\text{-}\omega}$ of 0.0241°, compared to 0.0090° for bulk Si(001) wafers. The peak broadening is primarily due to P-induced strain.

IV. DISCUSSION

We have shown that through their influence on θ_P, the deposition parameters $J_{P/Si}$ and T_s significantly affect the rate of Si(001):P layer growth from hydride precursors, the incorporation of P in the growing film, and surface morphological evolution. With increasing $J_{P/Si}$, R decreases, while C_P initially increases rapidly, and then begins to level off for $J_{P/Si} > 0.02$. Layers also roughen at higher PH_3 fluxes (T_s = constant) and T_s values ($J_{P/Si}$ = constant). These effects are due to the passivating nature of adsorbed P on Si(001) in concert with strong surface segregation. In this section, we discuss the kinetics of PH_3 adsorption, P surface segregation, and P incorporation in more detail. Kinetic rate equations are developed to describe our experimentally observed $\theta_P(T_s, J_{PH_3})$ and $C_P(T_s, J_{PH3})$ results.

A. PH_3 adsorption on Si(001)

PH_3 has been shown by high-resolution electron energy loss spectroscopy (HREELS) to dissociatively adsorb on Si(001) as PH_2 and H at 100 K, while the onset of PH_2 dissociation to adsorbed P and two H adatoms occurs at $T_s > 225$ °C.[13] The overall PH_3 adsorption reaction can, therefore, be expressed as

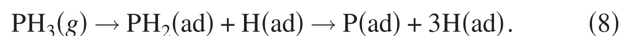

$$PH_3(g) \rightarrow PH_2(\text{ad}) + H(\text{ad}) \rightarrow P(\text{ad}) + 3H(\text{ad}). \quad (8)$$

TPD measurements show that phosphorus and hydrogen desorptions from Si(001) both recombinatively occur, by following second-order desorption kinetics, as P_2 and H_2. The onset temperature for P_2 desorption is ~600 °C with a rate constant $k_{d,P_2} = 4.2 \times 10^{11} \exp(-2.64 \text{ eV}/kT_s)$,[23] while the H_2 desorption onset temperature is ~400 °C [see Fig. 1(b)] with $k_{d,H_2} = 1 \times 10^{15} \exp(-2.52 \text{ eV}/kT_s)$.[10]

The saturation P coverage on Si(001) at a given T_s is dependent on the incident PH_3 flux J_{PH_3} and reactive sticking coefficient S_{PH_3}, the P_2 desorption rate, and the H surface coverage θ_H. There is a mutual interdependence between θ_P and θ_H; surface H inhibits PH_3 adsorption by terminating surface dangling bond sites. The time rates of change in θ_P and θ_H as a function of T_s can be expressed as

$$\frac{d\theta_P}{dt} = \frac{J_{PH_3} S_{PH_3}}{N_s}(1 - \theta_P - \theta_H)^2 - k_{d,P_2}\theta_p^2 \quad (9)$$

and

$$\frac{d\theta_H}{dt} = \frac{3J_{PH_3} S_{PH_3}}{N_s}(1 - \theta_P - \theta_H)^2 - k_{d,H_2}\theta_H^2, \quad (10)$$

where N_s is the surface site density, which is 6.8×10^{14} cm^{-2}. S_{PH_3}, which is the reactive sticking probability of PH_3 on clean Si(001), has been shown to be unity at room temperature.[25] We expect that $S_{PH_3} = 1$ at $T_s > 300$ K, since the dissociative adsorption of PH_3 on clean Si(001) should more readily occur at higher temperatures. The solution to the coupled Eqs. (9) and (10) provides a good fit to our experimental $\theta_P(T_s)$ data, as shown in Fig. 11(a). $\theta_H = 0.75$ ML ($\theta_P = 0.25$ ML) at $T_s < 400$ °C. With increasing T_s, θ_H rapidly decreases due to the onset of H_2 desorption, resulting in a corresponding increase in θ_P, which reaches a maximum near 1 ML at $T_s \sim 550$ °C before decreasing at higher T_s as the P_2 desorption rate becomes significant.

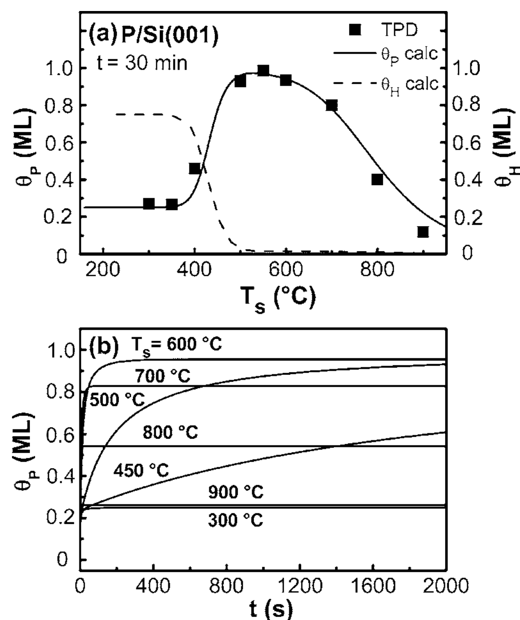

FIG. 11. (a) The data points are steady-state P coverages θ_P obtained from TPD measurements of Si(001) surfaces exposed to a PH_3 flux $J_{PH_3} = 1.65 \times 10^{14}$ cm^{-2} s^{-1} at temperatures T_s ranging from 300 to 900 °C. θ_P and θ_H curves are calculated by using Eq. (9) and (10). (b) Calculated results for θ_P as a function of PH_3 dosing time t with $J_{PH_3} = 1.65 \times 10^{14}$ cm^{-2} s^{-1}.

Calculated values of θ_P as a function of PH_3 exposure time t and dosing temperature are plotted in Fig. 11(b). At $T_s = 300$ °C, P_2 and H_2 desorption rates are slow and θ_P remains essentially constant at 0.25 ML. At $T_s = 450$ and 500 °C, θ_P slowly increases with dosing time but does not reach a steady-state value even at $t = 2000$ s (total PH_3 dose of 2.9×10^{17} cm^{-2}). With $T_s > 500$ °C, as H_2 desorption rates become increasingly fast, θ_P rapidly reaches steady state. Dosing times $t < 30$ s are sufficient at $T_s \geq 700$ °C. At a constant dosing time of 1800 s, θ_P initially increases with increasing T_s from a minimum of 0.25 ML at 300 °C to a maximum of 0.98 ML at 550 °C, before decreasing at $T_s > 600$ °C, reaching 0.26 ML at 900 °C.

B. P surface segregation during GS-MBE

The results presented in Sec. III B. for incorporated P concentrations C_P (Fig. 8) and surface coverages θ_P (Fig. 7) as a function of $J_{P/Si}$ and T_s during the growth of Si(001):P layers clearly demonstrate that P has a strong tendency toward surface segregation. Developing a predictive model for $C_P(J_{P/Si}, T_s)$ requires knowledge of the segregation enthalpy ΔH_s, since P is incorporated from the surface layer. The

Downloaded 07 Oct 2008 to 130.126.103.113. Redistribution subject to AIP license or copyright; see http://jap.aip.org/jap/copyright.jsp

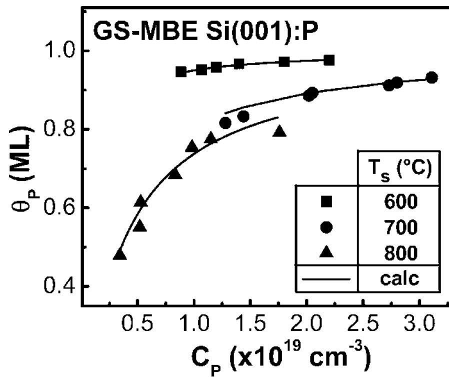

FIG. 12. The data points are steady-state P surface coverages θ_P as a function of the incorporated P concentrations C_P in GS-MBE Si(001):P layers grown with $J_{P/Si}$ ranging from 0.004 to 0.161 at T_s=600, 700, and 800 °C. Curves are calculated by using Eq. (12) with a P surface segregation enthalpy ΔH_s=−0.86 eV.

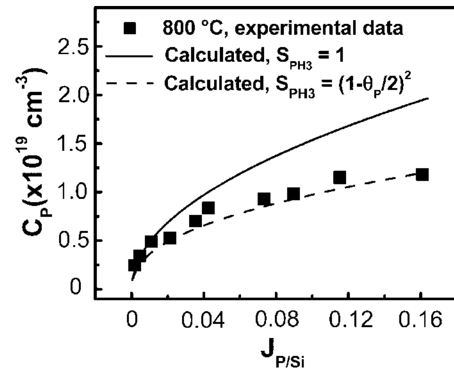

FIG. 13. The data points are experimentally determined P concentrations C_P in GS-MBE Si(001):P layers grown at T_s=800 °C as a function of the incident PH_3/Si_2H_6 flux ratios $J_{P/Si}$. $J_{Si_2H_6}$ was maintained constant at 2.1 $\times 10^{16}$ cm^{-2} s^{-1}. The curves are calculated from Eq. (14) by using PH_3 reactive sticking probabilities S_{PH_3} of 1 and $(1-\theta_P/2)^2$.

steady-state P segregation ratio during Si(001):P film growth, which is defined as the P surface coverage θ_P divided by the incorporated P fraction x_P, can be expressed as[26]

$$r_P = \frac{\theta_P}{x_P} = (1-\theta_P)\exp\frac{-\Delta H_s}{kT_s}. \tag{11}$$

Substituting the definition $x_P = C_P/n_{Si}$, in which n_{Si} is the bulk-Si atom density (5×10^{22} cm^{-3}), yields a direct relationship between θ_P and C_P,

$$\theta_P = \frac{C_P\exp(-\Delta H_s/kT_s)}{n_{Si} - C_P[1-\exp(-\Delta H_s/kT_s)]}. \tag{12}$$

To obtain ΔH_s, we combine the $\theta_P(J_{PH_3}, T_s)$ results obtained from TPD experiments [Fig. 11(a)] with $C_P(J_{PH_3}, T_s)$ data obtained from SIMS measurements (Fig. 8). For this analysis, we only use results from Si(001):P layers grown at $T_s \geqslant 600$ °C, for which θ_H is negligible and steady-state conditions are rapidly achieved [see Fig. 11(b)]. Figure 12 is a plot of θ_P versus C_P for layers grown at T_s=600–800 °C with $J_{P/Si}$ ranging from 0.004 to 0.161. At constant T_s, both C_P and θ_P increase with $J_{P/Si}$. An excellent fit to the experimental data is obtained by using Eq. (12) with a segregation enthalpy $\Delta H_s = -0.86 \pm 0.02$ eV. This is a reasonable value compared to results for other common *n*-type dopants, ΔH_s =−0.92 eV for Si(001):As (Ref. 11) and −1.2 eV for Si(001):Sb.[27] As and Sb are increasingly larger than P, which leads to higher strain-driven dopant segregation rates.

At sufficiently high film growth temperatures, P diffusion and segregation rates are much larger than film growth rates, which results in equilibrium segregation behavior, for which r_P increases with decreasing film growth temperature. If the film growth rate becomes of the order of, or greater than, the dopant segregation rate, segregation becomes kinetically limited and r_P increases with increasing T_s. The results in Fig. 12 show that with $T_s \geqslant 600$ °C, P surface segregation is in the equilibrium regime.

C. P incorporation kinetics

At constant Si(001):P growth temperatures $T_s \geqslant 600$ °C, incorporated P concentrations initially increase rapidly and then more slowly with increasing $J_{P/Si}$, as shown in Fig. 8. To obtain an expression for C_P as a function of T_s and $J_{P/Si}$ during Si(001):P gas-source epitaxy, we combine Eq. (12), which relates C_P to θ_P, with Eq. (9), which expresses the time rate of change of θ_P as a function of J_{PH_3}, S_{PH_3}, and T_s. At steady state, with T_s constant and $\theta_H \sim 0$ ($T_s \geqslant 600$ °C), Eq. (9) reduces to

$$\frac{J_{PH_3}S_{PH_3}}{N_s}(1-\theta_P)^2 = k_{d,P_2}\theta_p^2, \tag{13}$$

which, after rearranging, can be expressed as

$$\theta_p = \frac{\sqrt{J_{PH_3}S_{PH_3}}}{\sqrt{J_{PH_3}S_{PH_3}} + \sqrt{k_{d,P_2}N_s}}. \tag{14}$$

By combining Eqs. (12) and (14), and initially assuming S_{PH_3}=1, we obtain C_P versus. $J_{P/Si}$. Typical results are plotted in Fig. 13 for T_s=800 °C. Good agreement is obtained between the calculated curve and experimental data for layers with $C_P < 5\times 10^{18}$ cm^{-3}. However, at higher P doping concentrations, calculated C_P values are increasingly higher than the experimental data. We attribute this to a decrease in S_{PH_3} due to the lower dangling bond densities associated with increased θ_P. However, this is partially offset by the presence of P-induced surface defects, which increase θ_{db}. Surface defects play a significant role in adsorption, as discussed in Sec. III A, and must be accounted for when describing P adsorption and incorporation kinetics. Assuming that the majority of surface P is present in the form of Si—P dimers and that dissociative adsorption of PH_3 follows second-order kinetics, we express S_{PH_3} as $(1-\theta_P/2)^2$, where the factor of 2 in the denominator accounts for excess dangling bonds due to P-induced defects, as discussed in Sec. III A. This provides a good fit to the complete set of experimental data, as shown in Fig. 13.

Based on the above results, we conclude that the reason for the increasingly sublinear behavior of C_P with increasing $J_{P/Si}$ at constant T_s is the increase in θ_P, driven by strong P surface segregation, which gives rise to a decrease in the effective PH_3 sticking probability. Similar results have been reported for Si(001):As hydride growth.[11] Because of the de-

Downloaded 07 Oct 2008 to 130.126.103.113. Redistribution subject to AIP license or copyright; see http://jap.aip.org/jap/copyright.jsp

pendence of S_{PH_3} on θ_P, the overall P incorporation probability is extremely sensitive to the segregation rate. For example, Eqs. (12) and (14) show that decreasing r_P by 15% with $J_{P/Si}=0.001$ at $T_s=800$ °C increases C_P by ~60%.

D. Si(001):P surface morphological evolution

The observed changes in surface morphology and roughness w with T_s and $J_{P/Si}$ are directly related to the coverage and spatial distribution of P. In addition to dangling bond passivation, P adsorption induces ejection of surface Si atoms. Si ejection dominates at low θ_P values (i.e., low $J_{P/Si}$), which give rise to relatively smooth layers decorated with small Si islands. With increasing θ_P (as $J_{P/Si}$ is increased at constant T_s), P clustering and reductions in θ_{db} play a more significant role as film growth is inhibited at P-terminated surface sites and Si deposition preferentially occurs on P-free regions, causing laterally nonuniform layer growth, pitting, and an increase in roughness. The variation in surface morphology with T_s provides insight into the interdependent effects of P coverage and clustering on Si(001):P morphological evolution. At constant $J_{P/Si}$, θ_P reaches a maximum at $T_s \sim 550$ °C and decreases with increasing T_s, as discussed in Sec. III A. The high pit density, small average pit size, and relatively low roughness of films grown at 600 °C are indicative of a random distribution of surface P and high θ_P. With increasing $T_s > 600$ °C, thermally enhanced P surface mobilities lead to an increase in the degree of P clustering which, in conjunction with a decrease in θ_P due to P_2 desorption, results in larger average pit sizes, lower pit densities, and higher w values.

Self-organized ⟨100⟩-oriented pit formation suggests that surface P tends to form clusters aligned along the ⟨100⟩ directions, presumably to minimize strain energy. ⟨100⟩ oriented arrays of strained islands have also been observed during the growth of SiGe/Si(001) (Ref. 28) and Ge/Si(001),[29] and calculations have shown that the total energy of arrays of coherently strained islands on the (001) surface of a cubic crystal is minimized when the islands are aligned along the elastically soft ⟨100⟩ directions.[30]

V. CONCLUSIONS

During Si(001):P layer growth, high surface P coverages resulting from a strong driving force for segregation significantly influence film growth kinetics, P incorporation, and morphological evolution. We have investigated the dependence of θ_P, R, C_P, and surface morphology on T_s and J_{PH_3}. *In situ* D_2 TPD measurements of PH_3-adsorbed Si(001) at T_s values between 300 and 900 °C show that at low temperatures, for which H_2 and P_2 desorptions are negligible, θ_P initially remains constant at ~0.25 ML due to dissociation of PH_3 into adsorbed P and three H adatoms. As T_s is raised above ~400 °C, $\theta_P(T_s)$ increases as H_2 desorption begins to be significant and additional adsorption sites become available. $\theta_P(T_s)$ reaches a maximum of ~1 ML at $T_s=550$ °C and then decreases with increasing $T_s > 600$ °C due to P_2 desorption.

For growth of epitaxial Si(001):P layers at constant $J_{P/Si}$, the steady-state θ_P value initially increases with increasing T_s and then decreases with $T_s > 600$ °C, which is similar to the case of P adsorption. For example, with $J_{P/Si}=0.004$, θ_P varies from 0.25 ML at $T_s \leq 500$ °C, to a maximum of 0.54 ML at 600 °C, to 0.19 ML at 900 °C. With $J_{P/Si}$ constant, the incorporated P concentration C_P also increases with T_s, reaches a maximum, and decreases for $T_s > 700$ °C. A doping level of $C_P=3.1\times10^{19}$ cm^{-3} is obtained with $J_{P/Si}=0.142$ and $T_s=700$ °C. At constant T_s, C_P initially increases rapidly with $J_{P/Si}$ and then levels off at high flux ratios due to a decrease in the PH_3 sticking probability at high θ_P values.

The strong surface segregation of P during Si(001) film growth is demonstrated by comparing $\theta_P(T_s)$ and $C_P(T_s)$ results. Measured $\theta_P(T_s)$ values are much higher than would be expected from $C_P(T_s)$ data in the absence of segregation, by up to a factor of almost 3000. Such high surface phosphorus concentrations inhibit local film growth and result in surface roughening due to the passivating nature of P. As a result, R decreases as $J_{P/Si}$ (and thus, θ_P) increases at constant T_s. However, R increases with T_s at constant $J_{P/Si}$ due to exponentially faster H_2 and P_2 desorption rates. Fitting our $\theta_P(T_s, J_{PH_3})$ versus $C_P(T_s, J_{PH_3})$ data by using Eq (13) yields a P surface segregation enthalpy $\Delta H_s=-0.86$ eV.

Solving coupled equations for the θ_P and θ_H time rates of change, which are dependent on J_{PH_3} and T_s, yields an expression for $\theta_P(T_s, J_{PH_3})$ in excellent agreement with experimental data. We then insert $\theta_P(T_s, J_{PH_3})$ into Eq. (13) and obtain an expression for $C_P(T_s, J_{PH_3})$, which also exhibits good agreement with our experimental results and shows that, due to the interaction between θ_P and S_{PH_3}, the overall P incorporation probability is extremely sensitive to the P surface segregation rate.

Si(001):P surface morphology exhibits a pronounced dependence on $J_{P/Si}$ and T_s via changes in θ_P and kinetic limitations on adatom mobilities that affect the spatial distribution of surface P. As $J_{P/Si}$ increases at constant T_s, pitting becomes more pronounced due to higher P coverage and films become rougher. With increasing T_s at constant $J_{P/Si}$, pits become larger and the overall surface morphology dramatically changes, from a spongelike surface composed of a high density of small and randomly oriented pits to a surface with large pits and trenches aligned along the elastically soft ⟨100⟩ directions. This change in surface morphology with increasing T_s is due to a decrease in θ_P in conjunction with enhanced P adatom mobilities.

ACKNOWLEDGMENTS

The authors gratefully acknowledge the financial support of the U.S. Department of Energy (DOE), under Grant No. DEFG02-91ER45439 through the University of Illinois Frederick Seitz Materials Research Laboratory (FS-MRL). We also appreciate the use of the DOE supported MRL Center for Microanalysis of Materials (CMM) at the University of Illinois.

[1]E. Friess, J. Nützel, and G. Abstreiter, Appl. Phys. Lett. **60**, 2237 (1992).
[2]H. Hirayama and T. Tatsumi, Appl. Phys. Lett. **55**, 131 (1989).
[3]S.-M. Jang, K. Liao, and R. Reif, Appl. Phys. Lett. **63**, 1675 (1993).
[4]J. P. Liu, D. D. Huang, J. P. Li, D. Z. Sun, and M. Y. Kong, J. Cryst. Growth **200**, 613 (1999).

Downloaded 07 Oct 2008 to 130.126.103.113. Redistribution subject to AIP license or copyright; see http://jap.aip.org/jap/copyright.jsp

[5]F. Hirose, J. Cryst. Growth **212**, 103 (2000).
[6]Q. Lu, T. R. Bramblett, N.-E. Lee, M.-A. Hasan, T. Karasawa, and J. E. Greene, J. Appl. Phys. **77**, 3067 (1995).
[7]X.-J. Zhang, G. Xue, A. Agarwal, R. Tsu, M.-A. Hasan, T. Karasawa, and J. E. Greene, J. Vac. Sci. Technol. A **11**, 2553 (1993).
[8]T. R. Bramblett, Q. Lu, T. Karasawa, M.-A. Hasan, and J. E. Greene, J. Appl. Phys. **76**, 1884 (1994).
[9]H. Kim, G. Glass, T. Spila, N. Taylor, S. Y. Park, J. R. Abelson, and J. E. Greene, J. Appl. Phys. **82**, 2288 (1997).
[10]H. Kim, G. Glass, S. Y. Park, T. Spila, N. Taylor, J. R. Abelson, and J. E. Greene, Appl. Phys. Lett. **69**, 3869 (1996).
[11]H. Kim, G. Glass, J. A. N. T. Soares, P. Desjardins, and J. E. Greene, J. Appl. Phys. **88**, 7067 (2000).
[12]Y. Wang, X. Chen, and R. J. Hamers, Phys. Rev. B **50**, 4534 (1994).
[13]M. L. Colaianni, P. J. Chen, and J. T. Yates, Jr., J. Vac. Sci. Technol. A **12**, 2995 (1994).
[14]M. L. Yu, D. J. Vitkavage, and B. S. Meyerson, J. Appl. Phys. **59**, 4032 (1986).
[15]P. A. Redhead, Vacuum **12**, 203 (1962).
[16]F. M. Lord and J. S. Kittelberger, Surf. Sci. **43**, 173 (1974).
[17]U. Höfer, L. Li, and T. F. Heinz, Phys. Rev. B **45**, 9485 (1992).
[18]J. J. Boland, J. Vac. Sci. Technol. A **10**, 2458 (1992).
[19]H. Kim, P. Desjardins, J. R. Abelson, and J. E. Greene, Phys. Rev. B **58**, 4903 (1998).
[20]S.-S. Ferng, C.-T. Lin, K.-M. Yang, D.-S. Lin, and T.-C. Chiang, Phys. Rev. Lett. **94**, 196103 (2005).
[21]Y. Yang, M. J. Bronikowski, and R. J. Hamers, J. Phys. Chem. **98**, 5966 (1994).
[22]L. Kipp, R. D. Bringans, D. K. Biegelsen, J. E. Northrup, A. Garcia, and L.-E. Swartz, Phys. Rev. B **52**, 5843 (1995).
[23]M. L. Jacobson, M. C. Chiu, and J. E. Crowell, Langmuir **14**, 1428 (1998).
[24]K. A. Bratland, Y. L. Foo, J. A. N. T. Soares, T. Spila, P. Desjardins, and J. E. Greene, Phys. Rev. B **67**, 125322 (2003).
[25]B. S. Meyerson and M. L. Yu, J. Electrochem. Soc. **131**, 2366 (1984).
[26]J. E. Greene, S. A. Barnett, and A. Rockett, Appl. Surf. Sci. **22/23**, 520 (1985).
[27]S. A. Barnett and J. E. Greene, Surf. Sci. **151**, 67 (1985).
[28]T. Spila, P. Desjardins, A. Vailionis, H. Kim, N. Taylor, D. G. Cahill, J. E. Greene, S. Guillon, and R. A. Masut, J. Appl. Phys. **91**, 3579 (2002).
[29]B. Cho, T. S. Selinger, K. Ohmori, D. G. Cahill, and J. E. Greene, Phys. Rev. B **66**, 195407 (2002).
[30]V. A. Shchukin, N. N. Ledentsov, P. S. Kop'ev, and D. Bimberg, Phys. Rev. Lett. **75**, 2968 (1995).

Downloaded 07 Oct 2008 to 130.126.103.113. Redistribution subject to AIP license or copyright; see http://jap.aip.org/jap/copyright.jsp